6-13-2017

Jump Linear Quadratic Control for Energy Management of an Isolated Microgrid

Nathaniel Tucker
Santa Clara University, ntucker@scu.edu

SANTA CLARA UNIVERSITY

Department of Electrical Engineering

I HEREBY RECOMMEND THAT THE THESIS PREPARED
UNDER MY SUPERVISION BY

Nathaniel Tucker

ENTITLED

Jump Linear Quadratic Control for Energy Management of an Isolated Microgrid

BE ACCEPTED IN PARTIAL FULFILLMENT OF THE REQUIREMENTS
FOR THE DEGREE OF

MASTER OF SCIENCE
IN
ELECTRICAL ENGINEERING

Thesis Advisor – Dr. Maryam Khanbaghi	06/16/17 date
Thesis Reader – Dr. Aleksandar Zecevic	06/13/17 date
Department Chair – Dr. Shoba Krishnan	6/13/17 date

Jump Linear Quadratic Control for Energy Management of an Isolated Microgrid

By

Nathaniel Tucker

MASTER'S THESIS

Submitted to
the Department of Electrical Engineering

of

SANTA CLARA UNIVERSITY

in Partial Fulfillment of the Requirements
for the degree of
Master of Science in Electrical Engineering

Santa Clara, California

Spring 2017

Table of Contents

List of Figures

Jump Linear Quadratic Control for Energy Management of an Isolated Microgrid

Nathaniel Tucker

Dept. of Electrical Engineering, Santa Clara University, Santa Clara, CA, USA

ntucker@scu.edu

***Abstract*— Energy security and the aging grid infrastructure in the United States are two important subjects at the crossroads between politics and technology. One proposed solution to these two issues revolves around the concept of an *isolated microgrid*. Isolated microgrids are becoming increasingly popular combining multiple energy generation and storage systems to diversify and secure their private energy portfolios. The work presented in this thesis applies jump linear quadratic control to the energy management of an isolated microgrid operating with solar generation, fuel cell, and battery energy storage system. A continuous finite state Markov chain is used to model the intermittent generation of the solar array. The microgrid's energy management state-space is formulated, optimal feedback gains are calculated through a numerical algorithm, and results from an example system illustrate the validity of the proposed approach.**

I. INTRODUCTION

With prices of consumer photovoltaic (PV) generation systems decreasing, the number of small-scale electricity generating households is growing steadily. Specifically in California, where the weather is advantageous for solar generation, average citizens are installing PV generation systems at an impressive rate [1]. While this is a positive development that will help migrate energy production away from centralized fossil fuel plants by increasing the customers' control of their own electricity generation, many current household generation systems are not able to take full advantage of the electricity they generate. Households solely equipped with PV systems can only generate electricity when there is sun (daytime) and are forced to purchase electricity from the grid otherwise. Additionally, excess generated energy has to be sent back into the grid, instead of being stored for later use, which may negatively affect grid stability.

To circumvent this set of problems, several energy storage systems have emerged within the market that give households the ability to store self-generated energy for later use. These battery energy storage systems (BESS) facilitate several beneficial functions such as solar self-consumption, time of use load shifting, backup power, and off-the-grid use. With the increasingly common partnership of PV generation and battery energy storage systems, a household with both can be treated as its own microgrid system, capable of self-generation, storage, and only using a connection to the existing utility network when absolutely necessary. Control strategies for energy

management in microgrids have been studied in detail (see, *e.g.,* [2], [3], [4], [5], [6]), but most assume the microgrid has access to the public distribution grid to satisfy the load when the microgrid is unable to. For example, [4] focuses on the control and regulation of power characteristics at a point-of-common-coupling (PCC) between the microgrid and distribution grid. Another group of factors worth examining is the energy storage and generation technologies used in these systems. In [2], wind power is utilized as the primary stochastic resource; however, wind turbines are not a cost effective form of generation for small-scale microgrids. Similarly, [6] proposes a diverse portfolio of storage systems including large pumped-hydro plants. These gravity driven energy storage systems are too large and expensive for a one-home microgrid. Furthermore, [3] and [5] focus on multi-load systems utilizing shared resources with the goal of lowering overall energy cost.

The control strategy proposed in this thesis focuses on small off-the-grid systems; therefore, it does not have to handle multiple loads nor does it need to control competition for a shared resource. We are utilizing a control strategy and programming implementation that, to the best of our knowledge, has not been applied to an energy management problem. We believe the energy management problem of an isolated microgrid matches well with the characteristics of a jump linear system [7]. As such, we chose not to take a dynamic-programming (DP) approach as seen in [2] and [4]. Instead, we are utilizing a continuous Monte-Carlo simulation with discrete breaks at jump events. Also, we chose to forgo a connection to the grid and instead utilize a proxy distributed generation source, a hydrogen fuel cell. We made this decision not out of convenience, but to further support the concept of relinquishing power generation and distribution responsibilities from the public grid and giving the consumer complete control. A more recent work, [8], also utilized a Markov jump process in conjunction with energy storage systems; however, the work focused on inverter control instead of power balance and energy management. In the present work, our goal was to apply a specific control strategy to an isolated microgrid system equipped with a PV array, fuel cell, and battery to determine if average household microgrids can operate autonomously from the main grid with current technology available in the market.

In this thesis, we follow the controller design approach presented in [9], applying it to the energy management problem of our microgrid system. Section II describes our system architecture as well as specifics for each component. In Section III, jump linear quadratic control is introduced and applied to our microgrid system and section IV presents an example system with simulated results showing the effectiveness of the proposed strategy. In the final section, we make concluding remarks regarding implementation and future work.

II. System Description and Modeling

A. Microgrid Architecture

The microgrid system we are working with is represented in Figure 1. The system is equipped with a photovoltaic array for generation during the daytime, a hydrogen fuel cell for baseline energy generation, and a battery energy storage system acting as a buffer to smooth intermittent

generation and to optimize the energy generation/usage balance at night. Note that there is no connection to the standard utility power distribution network. This is an islanded microgrid that must self-generate all the load's required energy. For this reason, we treat it as an *isolated* microgrid.

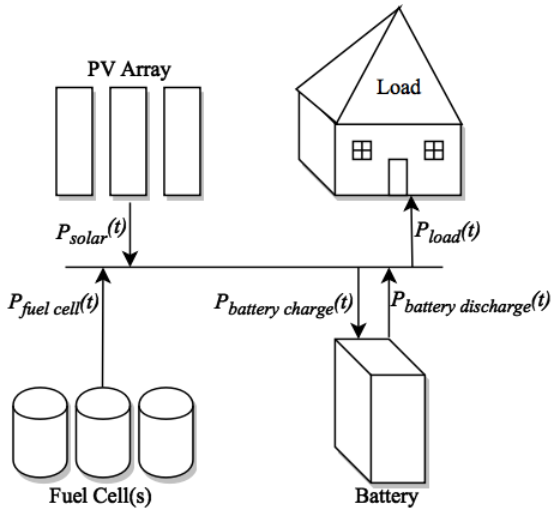

Fig. 1. Microgrid architecture with battery, fuel cell, solar, and load.

The primary goal of the system presented in this thesis is to manage the energy demand of a single home without being connected to the grid. This is done by balancing the power generated by the PV array, fuel cell, and battery with the power required by the load as:

$$P_{load}(t) = P_{solar}(t) + P_{fuelcell}(t) + P_{batt.\ discharge}(t) - P_{batt.\ charge}(t). \quad (1)$$

The power required by the load, $P_{load}(t)$, follows a preassigned trajectory described in the next section. Power generated by the PV array, $P_{solar}(t)$, follows a stochastic Markov chain process that depends on cloud coverage as well as time of day. The fuel cell's generated power, $P_{fuelcell}(t)$, is limited to discrete values depending on the generation capabilities of the specified fuel cell (the modular fuel cell selected for this implementation is described in *Subsection D*). Lastly, the battery can inject power into the system, $P_{batt.\ discharge}(t)$, as well as absorb power, $P_{batt.\ charge}(t)$.

The PV array should be sized in a way that is proportional to the daytime load of the house, to allow for full load satisfaction during sunny weather with the excess energy being sent to the battery. Likewise, it is desired for the fuel cell to act as a baseline generator and produce a constant amount of energy without the need to cycle between on and off states frequently. As stated before, the battery will act as the buffer which will accommodate the use of stored solar energy when the PV array is not producing energy. The load is modeled after an average house in the U.S. with additive noise for slight fluctuations in energy demand. The following assumptions are made throughout the thesis:

- In order to design the jump linear quadratic controller, the system operator has full information on the state of the system including instantaneous power flow, maximum and

minimum generation levels, as well as maximum and minimum battery levels. This would be implemented with a battery state-of-charge (SOC) tracker combined with voltage, current, or phasor monitoring devices.

- Reactive power is not taken into account. It is assumed that the controllers/inverters on the PV array, battery, and fuel cell regulate voltage and the phase angle. Only active power is considered.
- The operation of the fuel cell is simplified. The source of hydrogen and oxygen fuel is not specified and no energy is used for electrolysis, compression, or generation.

B. Load Model

The load in the isolated microgrid is modeled after an average house in the United States. The load consumption model comes from a National Renewable Energy Laboratory (NREL) System Advisor Model (SAM) dataset available online [10]. We took the NREL SAM data, $P_{base\ load}(t)$, and added zero-mean white Gaussian noise, $\omega_{load\ noise}(t)$, to get a load profile that follows a preassigned trajectory with stochastic variations in order to account for random changes in consumption. The power required by the load can be written as

$$P_{load}(t) = P_{base\ load}(t) + \omega_{load\ noise}(t). \tag{2}$$

Figure 2 presents a 72-hour selection of the load model. The goal of the microgrid energy management controller is to match this load through solar generation, fuel cell generation, and battery discharge.

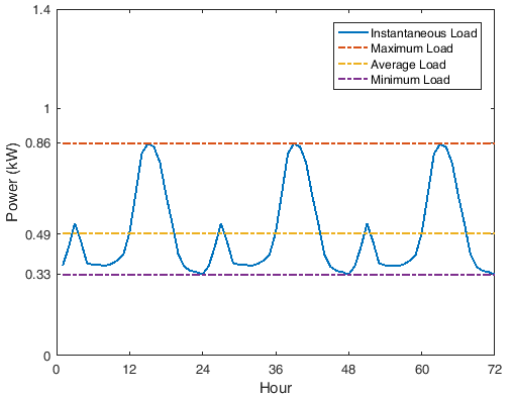

Fig. 2. 72 hour load profile for average U.S. residential home.

C. Solar Generation Model

Photovoltaic (PV) panels have been used for many years to convert energy from the sun into usable electric current through the photovoltaic effect. Solar power is becoming a highly coveted form of generation due to its passive generation profile and decreasing panel costs. However, solar generation possesses an intrinsic shortcoming which stems from the intermittent nature of meteorological systems. PV generation requires sunny weather for max efficiency, and generation

is severely obstructed by cloud coverage. To model this stochastic generation, a continuous Markov chain was used to represent cloud coverage patterns similar to the approach taken in [11].

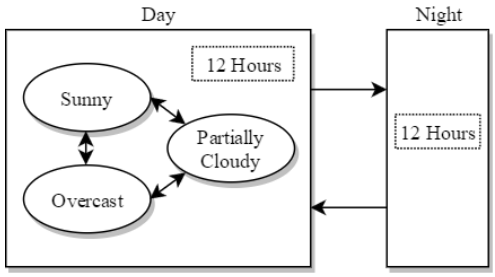

Fig. 3. Weather diagram with a Markov chain representing cloud coverage during daytime.

As seen in Figure 3, cloud coverage falls into one of three categories during the day: sunny, partially cloudy, and overcast. At night there is no generation since no solar radiation reaches the PV array. Consequently, the power generated by the PV array can be represented:

$$P_{solar}(t) = \begin{cases} P_{solar}^{day}(t) = \begin{cases} a, & r(t) = 1 \quad \text{(Sunny)} \\ b, & r(t) = 2 \quad \text{(Partially Cloudy)} \\ c, & r(t) = 3 \quad \text{(Overcast)} \end{cases} \\ P_{solar}^{night}(t) = 0 \end{cases} \tag{3}$$

where a, b, and c are static power values that are related to the number of panels, efficiency, and load requirements. The term, $r(t)$ denotes the mode of the Markov chain and is a discrete value from the set $S = \{1,2,3\}$ corresponding to the cloud coverage determined by a continuous Markov process for hours during the day, and a deterministic switch to $P_{solar}^{night}(t) = 0$ for the duration of night. The properties of this Markov process will be discussed further in Section III.

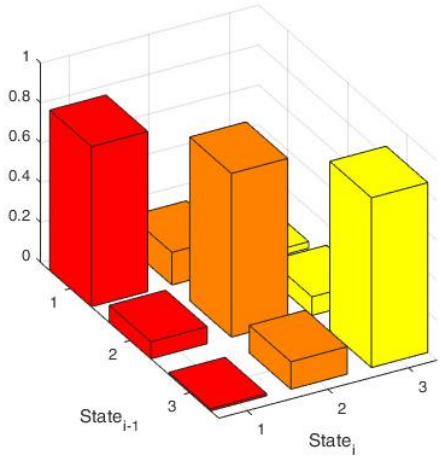

Fig. 4. Graphical representation of cloud coverage transition probability matrix.

Data for the cloud coverage transition probability matrix was gathered from San Jose International Airport's routine meteorological weather reports [12], also known as METAR.

METAR data is collected at all major airports and government buildings in the United States and specifies temperature, precipitation, as well as cloud coverage. For our purposes, the hourly cloud coverage data from 2016 was quantized into three levels: sunny, partially cloudy, and overcast and the transition rates were calculated in the manner shown in Figure 4. It is interesting to note how the magnitudes of the main diagonal compare to the off-diagonal elements in the transition matrix. It is evident that the cloud coverage system has a strong tendency to remain in one state for long periods of time. These long stretches of continuous weather are clearly consistent with California's stable weather patterns.

D. Battery Energy Storage

To supplement the intermittent generation from the PV array, a battery energy storage system is employed alongside a baseline fuel cell generator. The fuel cell is used to provide energy to satisfy a portion of the load that the solar and battery cannot. The battery essentially acts as a buffer, storing excess solar and fuel cell energy for later use. The effectiveness of this fuel cell and battery combination has been demonstrated in [13]. The important specifications of the battery include energy capacity, charge/discharge powers, life cycle, as well as safe operating temperatures. In our system, the battery has energy limits, $\underline{E}_b \leq E_b(t) \leq \overline{E}_b$, alongside charging and discharging limits, $0 \leq P_b^{ch.}(t) \leq \overline{P}_b^{ch.}$, $0 \leq P_b^{dis.}(t) \leq \overline{P}_b^{dis.}$, where $\overline{P}_b^{ch.}$ and $\overline{P}_b^{dis.}$ are the maximal allowable charge and discharge rates, respectively, for the specified battery. The derivative of the current energy stored in the battery can be expressed as

$$\frac{dE_b(t)}{dt} = P_b^{ch.}(t) - P_b^{dis.}(t) \tag{4}$$

where $P_b^{ch.}(t) = P_{solar}^{ch.}(t) + P_{FC}^{ch.}(t)$. For normal battery operation, it is common to set $\underline{E}_b \geq 10\%$ and $\overline{E}_b \leq 90\%$ of the maximum energy that can be stored to increase the lifespan of the battery.

E. Fuel Cell

Fuel cells are distributed generators that require compressed oxygen and hydrogen to generate electricity through continuous chemical reactions. Usually, fuel cells are paired with electrolyzers to split water molecules into oxygen and hydrogen for continual replenishment of the fuel cell. Fuel cells are effective generators for long periods of time, from several minutes up to several months [13]. Because of that, we are using a hydrogen fuel cell for energy generation for the isolated microgrid system. Similar to the battery, the fuel cell has generation limits $0 \leq P_{FC}^{ch.}(t) \leq \overline{P}_{FC}^{ch.}$. In our model, we are not restricting the total amount of energy the fuel cell is capable of supplying over time, which means that there is an essentially limitless supply of hydrogen and oxygen to power the chemical reaction. An electrolyzer and constant water supply could easily support this assumption. Adding the electrolyzer to the microgrid load as well as active hydrogen/oxygen tank monitoring will be studied in further work.

The proposed fuel cell has a modular architecture. The fuel cell consists of several independent chemical reaction cells for generation. This allows us greater control over the power generated by the fuel cell. Since we propose multiple modes of operation, the power generated by the fuel cell can be modeled as

$$P_{FC}^{ch}(t) = \begin{cases} 0 & 0 \text{ cells operating} \\ \frac{d}{3} & 1 \text{ cell operating} \\ \frac{2d}{3} & 2 \text{ cells operating} \\ d & 3 \text{ cells operating} \end{cases} \quad (5)$$

where d is a constant power determined by the specifications on the given fuel cell. In general, it is desirable to limit the switching frequency between states, on and off. As a result, the microgrid system should allow the fuel cell to operate continuously providing the power specified without the need to cycle between on and off states.

III. Jump Linear Quadratic Control

A. Jump Linear Systems Overview

The state-space representation of a jump linear system has the form

$$\dot{x}(t) = A\big(r(t)\big)x(t) + B\big(r(t)\big)u(t); \quad x(t_o) = x_o \quad (6)$$

where $x(t) \in \mathbb{R}^n$ and $u(t) \in \mathbb{R}^m$ represent the plant state and input control vector, respectively. $A(r(t))$ and $B(r(t))$ are $n \times n$ and $n \times m$ matrices, respectively, where $r(t)$ denotes the current system mode determined by a finite state Markov jump process ($r(t)$ takes discrete values from a finite set $S = \{1,2, \dots N\}$ depending on how many modes of operation the system has). The system jumps between modes following probabilities given in the jump transition density matrix:

$$\Pi = (\pi_{ij}); \quad i,j = 1,2, \dots N$$

with

$$\pi_{ii} < 0; \quad \pi_{ij} > 0 \quad \text{for} \quad i \neq j$$

and

$$\sum_{j=1}^{N} \pi_{ij} = 0 \quad \text{for} \quad i = 1,2, \dots N.$$

When the system is operating in the *i*th mode, $r(t) = i$, the corresponding system matrices $[A\big(r(t)\big),\ B\big(r(t)\big)]\ |_{r(t)=i}$ will be denoted $[A_i, B_i]$. When designing an optimal controller for such a system, one aims to minimize the quadratic cost function

$$J(u, t_0, r(t_0), x_0) = \mathbf{E}\left\{\frac{1}{2}\int_{t_0}^{t_f}\Big(x^T(t)Q\big(r(t)\big)x(t) + u^T(t)R\big(r(t)\big)u(t)\Big)\,dt \mid t_0, r(t_0), x_0\right\}. \quad (7)$$

The weighting matrices, $Q\big(r(t)\big)$ and $R\big(r(t)\big)$, are mode dependent and are used to tune the system response to fit desired characteristics. In the following, they will be denoted as $[Q_i, R_i]$ with $Q_i \geq 0$ and $R_i > 0$ when the system is operating in its *i*th mode. The optimal controller has the form

$$u^*\big(x(t), r(t)\big) = -R_i^{-1} B_i^T K_i(t) x(t) \quad \text{for} \quad r(t) = i \tag{8}$$

where matrices $K_i(t)$ $(i = 1,2, \ldots N)$ satisfy the set of coupled differential matrix Riccati equations

$$\dot{K}_i = -A_i^T K_i - K_i A_i - Q_i + K_i S_i K_i - \textstyle\sum_{j=1}^{N} \pi_{ij} K_j \tag{9}$$

with $S_i = B_i R_i^{-1} B_i^T$ and $K_i\big(t_f\big) = 0$.

In the following, we will be interested in steady state values K_i. It is assumed that stochastic controllability and observability requirements are met. The corresponding algebraic Riccati equation (which was obtained using the variable transformation $\tilde{A}_i = (A_i + \left(\frac{1}{2}\right)\pi_{ii} I)$ presented in [14]) can be written as

$$\tilde{A}_i^T K_i^{\infty} + K_i^{\infty} \tilde{A}_i + Q_i - K_i^{\infty} S_i K_i^{\infty} + \textstyle\sum_{j=1, j\neq i}^{N} \pi_{ij} K_j^{\infty} = 0. \tag{10}$$

If the system is observable, (that is if $\big(\sqrt{Q_i}, A_i\big), 1 \leq i \leq N$ is observable) there exists a unique positive definite solution to equation (10) [14]. Using the first algorithm presented in [14], we can find the $K_i^{\infty}, 1 \leq i \leq N$ matrices for our optimal control actions from (8). It is worth noting that this is not the only feasible control strategy. We chose this approach because it readily accommodated the hybrid nature of our system. Other approaches will be the subject of future work.

B. JLQ Control Applied to Isolated Microgrid

The isolated, or islanded, microgrid system combines continuous system dynamics with discrete mode jumps every hour. This hybrid realization stems from the hourly weather condition jumps modeled by the Markov process described in Section II. The jump variable, $r(t) \in \{1,2,3\}$, corresponds to {*Sunny*, *Partially Cloudy*, *Overcast*} respectively. The Markov jump transition density matrix calculated from the METAR data [12] is

$$\Pi = \begin{bmatrix} -0.197 & 0.164 & 0.033 \\ 0.085 & -0.179 & 0.094 \\ 0.010 & 0.138 & -0.148 \end{bmatrix}. \tag{11}$$

A representative 96-hour segment from a Monte-Carlo simulation of the weather is shown in Figure 5. The system will operate in a continuous state with $[A_i, B_i]$; $r(t) = i$ for 1 hour until the next mode, $r(t) = j$, occurs. The system has unique state-space matrices, $[A_i, B_i]$, for each mode, $r(t)$, of the Markovian solar generation model which determine the proportions of power being sent to the load and battery from the PV array and fuel cell.

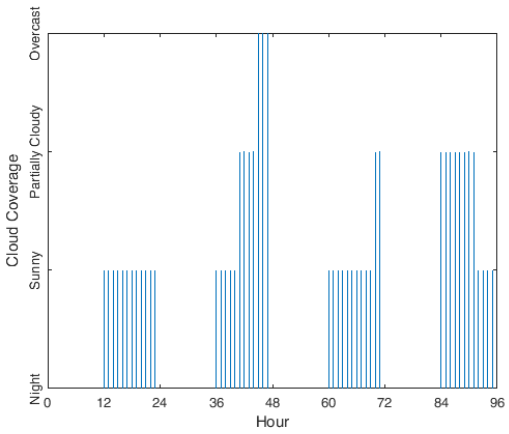

Fig. 5. 96-hour Markovian weather condition simulation with deterministic jumps to r(t) = night every 12 hours.

For example, during a sunny day, the PV array contributes most of its generated power to the load with the excess being sent to the battery while the fuel cell operates at a low generation level. The power balance equations (12) and (13) allow for the customization of scalar values a_i, b_i and c_i for each mode of operation, $i \in \{1,2,3,4\}$, corresponding to {*Sunny*, *Partially Cloudy*, *Overcast*, *Night*}. By designing our system equations in this way, we coupled each node in the system while abstracting its specific details.

$$\frac{dE_b(t)}{dt} = \alpha E_b(t) + (1 - a_i)P_{solar}^{ch.}(t) - b_i P_b^{dis.}(t) + (1 - c_i)P_{FC}^{ch.}(t) \tag{12}$$

$$\frac{dE_l(t)}{dt} = \beta E_l(t) + a_i P_{solar}^{ch.}(t) + b_i P_b^{dis.}(t) + c_i P_{FC}^{ch.}(t) \tag{13}$$

The terms $E_b(t)$ and $E_l(t)$ correspond to the energy stored in the battery and the energy required by the load, respectively. The scalar coefficients α and β take the appropriate units of $(\text{hour})^{-1}$ and are set equal to -1 for this analysis (which ensures that our derivative states depend on the current energy levels of the load and battery).

If we define the state variables, output variables, and input/control variables as

$$x(t) = \begin{bmatrix} E_b(t) \\ E_l(t) \end{bmatrix}, y(t) = \begin{bmatrix} E_b(t) \\ E_l(t) \end{bmatrix}, u(t) = \begin{bmatrix} P_{solar}^{ch.}(t) \\ P_b^{dis.}(t) \\ P_{FC}^{ch.}(t) \end{bmatrix} \tag{14}$$

the state-space representation becomes

$$\begin{aligned} \dot{x}(t) &= \begin{bmatrix} 1 & 0 \\ 0 & 1 \end{bmatrix} x(t) + \begin{bmatrix} 1 - a_i & -b_i & 1 - c_i \\ a_i & b_i & c_i \end{bmatrix} u(t) \\ y(t) &= \begin{bmatrix} 1 & 0 \\ 0 & 1 \end{bmatrix} x(t) + \begin{bmatrix} \omega_1(t) \\ \omega_2(t) \end{bmatrix} \end{aligned}, \; i \in \{1,2,3,4\} \tag{15}$$

where $\omega_1(t)$ and $\omega_2(t)$ represent noise. These two terms model the random variation of the load and show that the controller can handle noisy measurements. Once the values of a_i and b_i are chosen for each mode of operation, the optimal controller can be calculated as

$$u^*\big(x(t), r(t)\big) = -R_i^{-1} B_i^T K_i^{\infty} x(t) \quad \text{for} \quad r(t) = i \tag{16}$$

where K_i^{∞} is found using the algorithm proposed in [14]. It is important to note that since the system dynamics are inherently mode dependent, the control law is mode dependent as well. Consequently, the controller gains $K_i = -R_i^{-1} B_i^T K_i^{\infty}$ will remain the same in each mode.

IV. Example System And Results

A. Example System Specifications

In this section, we will consider a system that conforms to the model described in the previous section and examine the simulation results. For simulation purposes, the load data was sampled at hourly intervals and then held constant to produce a piecewise-continuous load profile. The load profile shown in Figure 6 (which follows the pattern shown in Figure 2) pertains to a small U.S. household, one similar in size and energy usage to common off-the-grid homes. The peak demand of $0.86\ kW$ occurs in the evening and the mean usage is $0.49\ kW$.

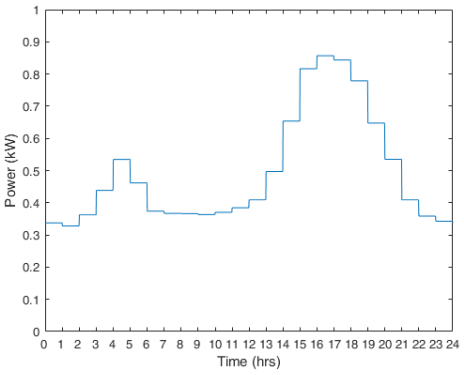

Fig. 6. Sampled daily load profile.

Among the components of the isolated microgrid, we identified the solar contribution as the most influential. We assumed that during a sunny day, the solar production completely satisfies the demand with some excess energy that can be stored in the battery for later use. Consequently, we chose the values $a = 0.6\ kW, b = 0.4\ kW,$ and $c = 0.3\ kW$ corresponding to sunny, partly cloudy, and overcast generation respectively for equation (3). The fuel cell was designed to satisfy the demand when the battery and solar could not. The fuel cell contributed a maximum of $P_{FC}^{ch.} = 0.35\ kW$ around 7:00pm when the load was still high from evening activity in the house. During a sunny day, the fuel cell was turned off since solar generation fully satisfied the demand. Lastly, for the household in this example, we employed a $7\ kWh$ battery and imposed capacity limits at $\underline{E_b} = 1\ kWh\ and\ \overline{E}_b = 6.5\ kWh$ to ensure maximum healthy lifetime of the device. The

maximum charge rate was $\overline{P}_b^{ch.} = 0.3\ kW$ and the maximum discharge rate was $\overline{P}_b^{dis.} = 0.35\ kW$. We provided the battery with an initial 50% state of charge corresponding to 3.5 kWh.

Once the components are sized appropriately for the given system, the power flow coefficients a_i, b_i and c_i from equations (12) and (13) can be selected to weight the contributions from solar, battery, and fuel cell. The values used in this case study are as follows:

$$\begin{aligned} &a_1 = 0.8, \quad b_1 = -1, \quad c_1 = 0.2, \quad r(t) = 1\,, sunny \\ &a_2 = 0.9, \quad b_2 = -1, \quad c_2 = 0.7, \quad r(t) = 2\,, partially\ cloudy \\ &a_3 = 0.9, \quad b_3 = 1, \quad\ \ c_3 = 0.9, \quad r(t) = 3\,, overcast \end{aligned}$$

This means that, when the weather is overcast, the load will receive 90% of the small amount of solar power generated and the battery gets the remaining 10%. Similarly, the load will receive 90% of the power from the fuel cell while the battery receives the other 10%. The battery will charge during periods of good weather and discharge when the weather is overcast (and at night, of course).

An item worth noting is the value of coefficient b_i that multiplies the battery discharge rate, $P_b^{dis.}(t)$, during sunny and partially cloudy conditions. Since there is excess solar generation during this time, the battery discharge is set to a negative value in order to induce charging. Given that there is no solar contribution during the 12 hours of night, the coefficient a_4 is multiplied by 0 (and is therefore irrelevant). The other coefficients during nighttime are $b_4 = 1\ and\ c_4 = 0.9$.

B. Monte Carlo Simulation Results

The example system was simulated for 5 days with cloud coverage generated from the continuous Markov process explained in Section II. In the following, we present results from a 5 day period that trended towards sunny days and another set of results from a 5 day period that trended towards overcast weather (this can be done due to the random permutations of weather generated from the Markov process each time the program is run). Figure 7 presents weather data with a large segment of overcast followed immediately by the deterministic jump to nighttime at hour 72. Apart from this one segment, the rest of the days are either sunny or partially cloudy.

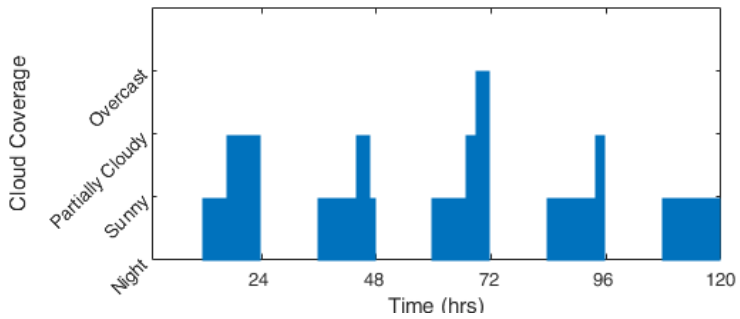

Fig. 7. 120 hour Monte-Carlo simulation with stretch of overcast weather and night combined.

Figure 8 shows the household load profile from Figure 6 alongside the simulated system response of the jump linear quadratic controller. During day 3 (when the overcast weather occurs) the controller successfully compensates for the decreased solar generation by discharging the battery to match the load.

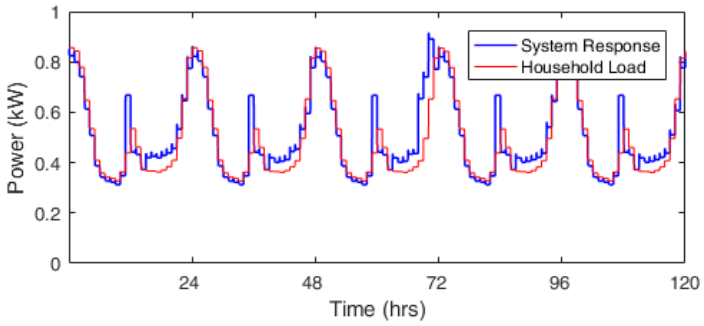

Fig. 8. System response with long overcast and night period.

Figure 9 shows the input control vector $u(t)$ obtained from equation (16). The solar generation is a stochastic variable following the Markovian process described earlier. Depending on the weather, solar generation takes a constant value for that hour. The battery power takes a negative value during sunny and partially cloudy weather, which indicates that the battery is charging. Likewise, when the battery and fuel cell generation values are positive, they are discharging to satisfy the demand. It should be noted that near hour 72 (when the weather switches to overcast) the battery stops charging and begins discharging to accommodate the decrease in solar generation at that time.

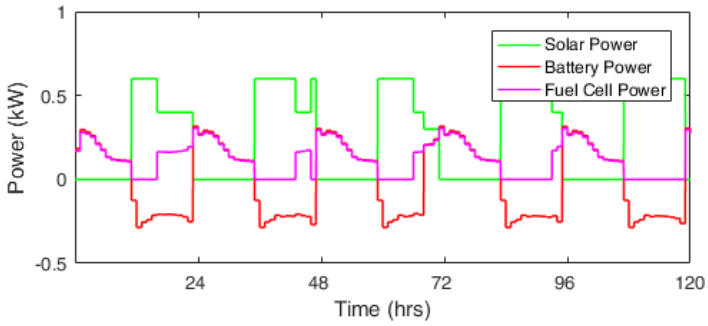

Fig. 9. Solar, battery, and fuel cell contributions (long overcast and night period).

The total amount of energy stored in the battery is shown in Figure 10 (the battery's maximum and minimum allowed levels are indicated by the horizontal lines). Around hour 84 (the end of night 4) the battery temporarily hits the lower limit. This is due to the long period of minimal solar generation (overcast) followed by 12 hours of no solar generation (night). However, the battery was able to recover during the next day, and its energy level remained above the minimal value during the following night.

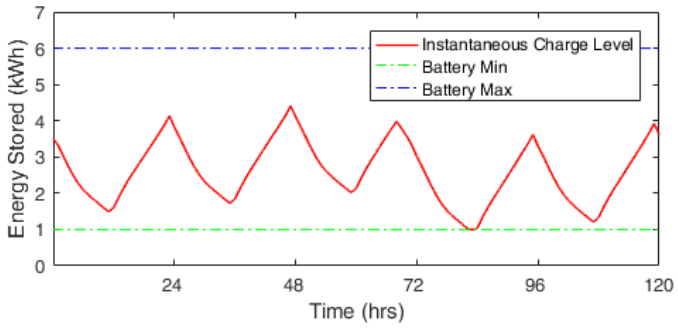

Fig. 10. Energy stored in the battery (long overcast and night period).

Figures 11-14 show simulation results for 5 days of mostly sunny weather. An item worth noting is the difference that occurs at hours 12, 36, 60, and 108 between the simulated system output compared to the household load profile in Figures 8 and 12. The controller consistently overshoots the actual load of the house for this hour. This is because of the deterministic jump from no solar generation (night) to medium or high solar generation (day). Due to the design of the controller to account for the stochastic nature of weather during the day, it is not well equipped to account for this deterministic jump point each day. One future solution we are looking into involves a two-level control strategy. The primary controller will account for average night and day contributions while the second level manages the stochastic daytime solar contributions. Further work will be done to refine the controller and account for this.

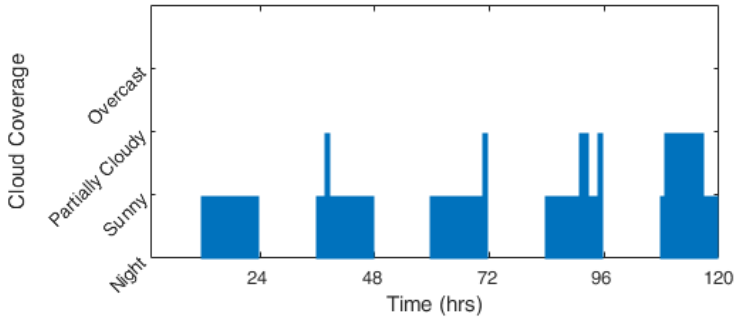

Fig. 11. 120 hour Monte-Carlo simulation with mostly sunny weather.

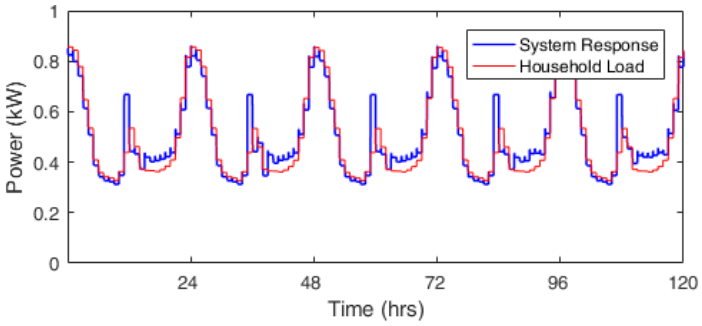

Fig. 12. System response with mostly sunny weather.

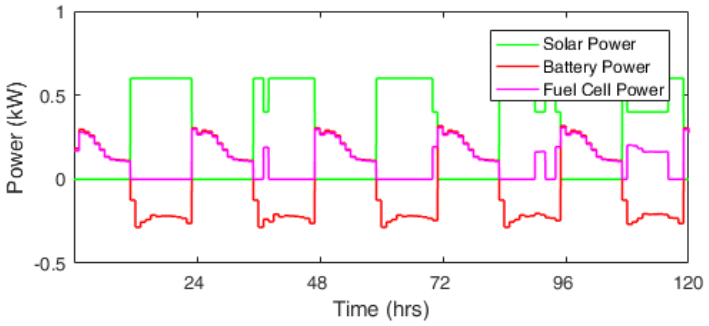

Fig. 13. Solar, battery, and fuel cell contributions (mostly sunny).

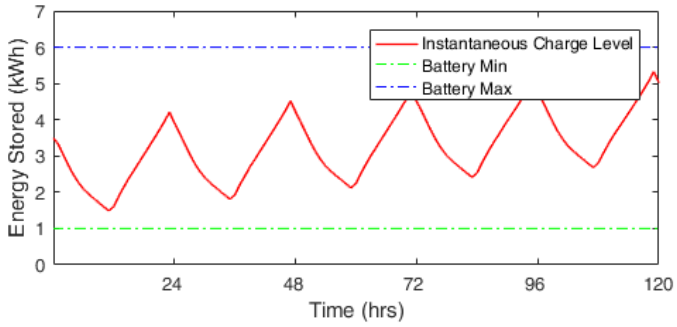

Fig. 14. Energy stored in the battery (mostly sunny).

Due to the mostly sunny weather of this 5 day simulation, the battery never reaches the minimum allowed charge level (as seen in Figure 14). The battery's total charge trends upward over the 5 day period and would reach full charge within another 2 days if the good weather were to continue.

V. Conclusion and Future Work

This thesis presents the application of jump linear quadratic control to the energy management problem of an isolated microgrid. The microgrid utilizes solar and fuel cell generation combined with a battery energy storage system to satisfy the load of a small household. The solar generation depends on a continuous Markov process that determines the cloud coverage with discrete jumps to night every 12 hours. The controller accounts for the continuous and discrete hybrid nature of the system by charging and discharging the battery accordingly.

Simulation results for an example system showed the effectiveness of the proposed control method to track the load profile of the house. The control method was able to accommodate the stochastic jumps between operation modes and satisfy the demand each night. This control scheme paired with the presented microgrid architecture proved to be a robust and efficient implementation for grid isolated operations. For the example system, a $7\,kWh$ battery and $0.35\,kW$ fuel cell proved to be large enough for the application. For any system following this design, we suggest utilizing a larger fuel cell, nearly double the required size, in case of longer periods of intemperate weather during winter seasons.

Future work could include more cloud coverage states in the Markov process to increase the granularity of the controller. Furthermore, other possible control strategies such model predictive control (MPC) could be applied to the system architecture.

Acknowledgment

The authors would like to thank Dr. Aleksandar Zecevic for his valuable comments and Santa Clara University School of Engineering for their support.

REFERENCES

[1] Residential Solar Statistics – California Solar Initiative (CSI), www.gosolarcalifornia.ca.gov

[2] A. Belloni, L. Piroddi, and M. Prandini, "A Stochastic Optimal Control Solution to the Energy Management of a Microgrid with Storage and Renewables," *2016 American Control Conference (ACC)*, Boston, MA, 2016, pp. 2340-2345.

[3] P. Dimitrov, L. Piroddi, and M. Prandini, "Distributed Allocation of a Shared Energy Storage System in a Microgrid," *2016 American Control Conference (ACC)*, Boston, MA, 2016, pp. 3551-3556.

[4] Y. Levron, J. M. Guerrero, and Y. Beck, "Optimal Power Flow in Microgrids with Energy Storage," *IEEE Trans. on Power Sys.*, vol. 28, no. 3, pp.3226-3234, Aug. 2013.

[5] H. Dagdougui, L. Dessaint, G. Gagnon, and K. Al-Haddad, "Modeling and Optimal Operation of a University Campus Microgrid," *2016 IEEE Power and Energy Society General Meeting (PESGM)*, Boston, MA, 2016, pp. 1-5.

[6] H. Dagdougui, R. Minciardi, A. Ouammi, M. Robba, and R. Sacile, "A Dynamic Decision Model for the Real-Time Control of Hybrid Renewable Energy Production Systems," *IEEE Systems Journal*, vol. 4, no. 3, pp. 323-333, Sept. 2010.

[7] M. Mariton, *Jump Linear Systems in Automatic Control*, New York, Marcel Dekker Inc., 1990.

[8] S. Liu; X. Wang; P. X. Liu, "A Stochastic Stability Enhancement Method of Grid-Connected Distributed Energy Storage Systems," in *IEEE Transactions on Smart Grid* , vol.PP, no. 99, pp. 1-9. January 2016.

[9] M. Khanbaghi, R. Malhamé, M. Perrier, "Optimal White Water and Broke Recirculation Policies in Paper Mills Via Jump Linear Quadratic Control," *IEEE Trans. on Control Systems Technology*, vol. 10, no. 4, July 2002.

[10] Residential Load Modeling – System Advisor Model (SAM), National Renewable Energy Laboratory (NREL), sam.nrel.gov

[11] D. Sworder, R. Rogers, "An LQ-Solution to a Control Problem Associated with a Solar Thermal Central Receiver," *IEEE Trans. on Automatic Control*, vol. AC-28, no. 10, Oct. 1983.

[12] Meteorological Aviation Routine Weather Reports (METAR/SPECI), San Jose International Airport (SJC), www.noaa.gov

[13] J. Barton, D. Infield, "Energy Storage and Its Use with Intermittent Renewable Energy," *IEEE Trans. on Energy Conversion*, vol. 19, no. 2, pp. 441-448, June, 2004.

[14] H. Abou-Kandil, G. Freiling, and G. Jank, "Solution and Asymptotic Behavior of Coupled Riccati Equations in Jump Linear Systems," *IEEE Trans. on Automatic Control*, vol. 39, no. 8, Aug. 1994.

[15] Ting, T., *et al*. "State-Space Battery Modeling for Smart Battery Management System," *Proc. Of the Int. MultiConference of Eng. And Comp. Sci. (IMECS),* vol. 2, 2014.

[16] Zhang, Y., *et al.* "Day-Ahead Smart Grid Cooperative Distributed Energy Scheduling with Renewable and Storage Integration," *IEEE Trans. On Sust. Energy*, vol. 7, no. 4, Oct. 2016.

[17] Camacho, E., *et al.* "Control for Renewable Energy and Smart Grids," *The Impact of Control Techonology*, www.ieeecss.org